ISR TECHNICAL REPORT 2008-9

Process Modeling of a Wire Saw Operation

Thomas Palathra, Raymond Adomaitis

ABSTRACT

Multicrystalline (MC) silicon solar cells are manufactured from bread-loaf sized ingots of solar-grade silicon. These ingots are sliced by a multi-wire saw mechanism consisting of a single thin and extremely long stainless steel wire wound on constant-pitch wire grooves. The wire is wound over each groove to create a web consisting of 500-700 parallel wires. The wire is kept at a constant tension using feedback control and the wire speeds typically are 10-15 m/s. A high speed nozzle directs an aqueous slurry of oil and SiC particles to the top of the wire array and the crystal silicon ingot is pushed upwards against the wire array during the cut. In a typical wire saw system, MC ingots are sliced with an area of 100x100 mm^2 and the latest wire saw systems can achieve thicknesses down to 300 μm.

What makes this a challenging simulation problem is the wide range of timescales that characterize the overall cutting process. The slowest dynamics are associated with the evolution of the cut, which is described by a spatially dependent differential equation in time and in which the cutting rate is modeled much in the same manner as the Chemical Mechanical Planarization (CMP) process. Cutting rate is a direct function of the distance between the wire and ingot surface. Because the wire dynamics are orders of magnitude faster than the cut evolution, the wire deflection is modeled by a static circular beam. The goal of this modeling work is to understand the physical mechanisms that limit how thin the wafers can be cut and to determine the sensitivity of cutting time and cutting rate based on process operating conditions.

Contents

List of Figures

List of Tables

Chapter 1

1 Introduction

1.1 Motivation

Photovoltaic (PV) materials and module processing industry has been a large focus for research for the last two decades because of the obvious desire for alternative energy. The projected total energy consumption in the year 2050 is projected to be 28 TW. Energy in the form of sunlight provides 14 TW in an hour so there is much to gain by converting this abundant source into a consumable source of energy. However, in 2007 it cost 30 cents kWh^{-1} to produce energy using PV technology and when compared with the 5-8 cents kWh^{-1} cost from conventional resources (coal, fossil fuels, natural gas) , economic hurdles still exist for commercial PV implementation. [1]

As with transistors and microprocessors, silicon is the main semiconductor material in PV cells. Purified polysilicon is melted and crystallized into cylindrical or rectangular ingots via either the Chocharlaski technique or the (MC) multi-crystalline technique. Figure 1 shows a typical MC ingot to be wafered. The square MC silicon wafers comprise 82 % of PV modules. [2,3] . The cost of PV modules and cells is proportional to the cost of solar grade crystalline polysilicon. [2] In 2003, 2004, and 2005 polysilicon costs were \$24 kg^{-1}, \$32 kg^{-1}, and \$45 kg^{-1}, respectively. [1] Due to this high demand and price, minimizing silicon lost to wafering and reducing the thickness of the wafer is imperative.

Figure 1: *A typical MC Ingot [4] NREL*

Figure 2: *An Ingot after being wafered by a wire saw. [4] NREL*

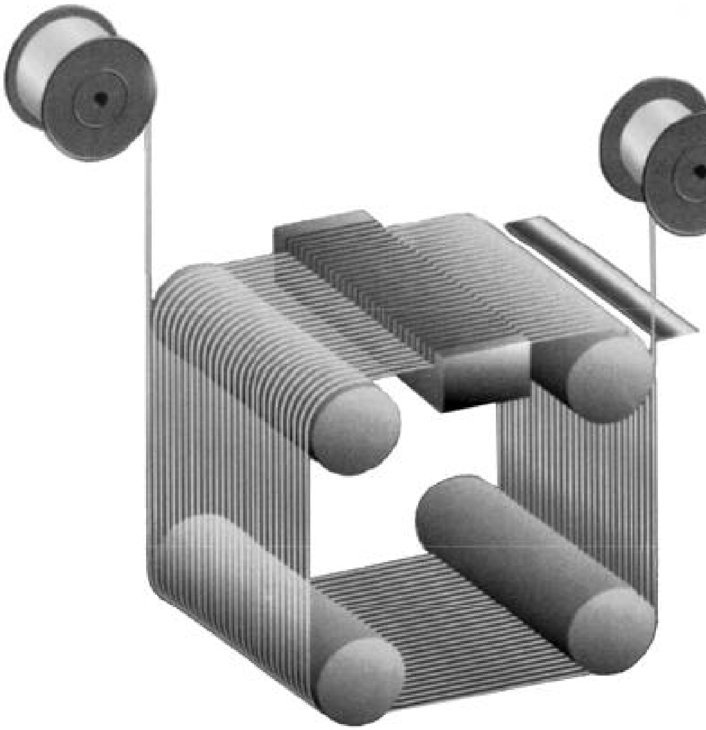

Figure 3: *An illustration of a wire saw setup from Möller et.al. [2]*

The ingot is wafered by a multi-wire saw and fig. 2 exhibits the ingot after being sawed. A typical wire saw setup is depicted in fig 3. The multi-wire saw mechanism consists of a single thin stainless steel wire fed from a supply spool and wound over constant-pitch wire grooves of a spindle. The wire is wound over each groove providing a wire web consisting of 500-700 parallel wires. The wire is kept at a constant tension of 20-50 N via feedback control and wire speed is maintained at 10-15 m/s [5,6]. A high speed nozzle feeds a slurry of oil and SiC particle abrasives onto the wire array and the crystal silicon ingot is pushed up against at a constant feed force. SiC abrasives are trapped against the wire and removes material from the normal force applied and the relative velocity. The role of the fluid is to transport material removed, to reduce friction, and to provide cooling.[5,6] The production of wafered silicon comprises between 40-60 % of the total solar cell production cost. The actual sawing technique comprises 30% of the wafer production. [7] SiC is a very expensive material that constitutes 25 % of the slicing cost [5] and the recovery of used SiC has not yet been executed efficiently. The wire saw technique has achieved wafers with thickness of 300 μm and with the goal to reduce thickness to 100 μm.

1.2 Past Work

Recent research on the wire saw has just started in the last decade. Fluid dynamics and the particle size distribution in the cutting channel has been shown to predict the cutting mode. Work done by Bhagavat et. al and Möller et. al have used lubrication theory to calculate the film thickness and the existing hydrodynamic pressure to subsequently calculate a removal rate. [5-7] By determining the scale of the film thickness either a free abrasive cutting or a solid-semi contact mode has been predicted. Li et. al have developed a model cutting model based on a conical abrasive and termed their material removal as a ”rolling and indenting removal”. [8] However none of these models looked at the transient behavior of the cutting rate nor have they captured the slow dynamics of the ingot profile evolution.

Also studies have been done to describe defects of the wafer as a result of wire saw wafering. Thermal warping of the wafer from the frictional heat has been modeled and is in good agreement with experimental studies. [9,10] In addition, hard inclusion defects in the silicon ingot have recently been investigated and shown to adversely effect the sawing process. [11] These agglomerates of hard particles are regions where the wire saw can not cut and possibly break the wire. Lastly, the common wavy surface finish that characterizes wire saw cuts has yet to be predicted effectively. [12]

1.3 Goals

To the knowledge of this researcher, only one other American group (SUNY Stony Brook) has developed wire saw models and experiments. Predominantly all wire saw research is based in Asia and Europe. One long-term goal is to develop a series of models and experiments to predict surface quality and determine factors to reduce wafer thickness.

Our goal in this project is to develop a novel model that couples the slow dynamics of the ingot cutting evolution and the fast dynamics of the cutting. Subsequently, cutting rates along the wire length, cutting time, and the sensitivity of these variables to process parameters will be determined.

Chapter 2

2 System Modeling

2.1 Base Case

The base case wire saw system, which is typical of wire saw applications is described as follows. From fig. 4, MC ingots are sliced with an area of 100 x 100 mm^2 and the spool to spool length, L, is typically 300 mm [5,6]. The latest wire saw system can achieve thickness down to 300 μm with a kerf of 200 μm utilizing a wire radius, R, of 80 μm. A constant tension, H, 20 N with a silicon ingot loading, F=1.7 N per wire are all values used in industry [6]. The wire is stainless steel with an elastic modulus, E=195 GPa and translating speed, U=10 m/s. Table 1 summarizes the parameters used in the base case.

Table 1: Base Case Parameters

Parameter	value
H	20N
U	10m/s
E	195GPa
R	80μm
F	1.7N/wire
A	100 x 100 mm ^{2}
L	300mm

2.2 Modeling Equations

The system is considered multiscaled because of the multiple time scales characterizing the cutting process. First, the evolution of the ingot profile is slowly changing, with a characteristic time on the order of hours. [13] The cutting process is modeled by a Chemical

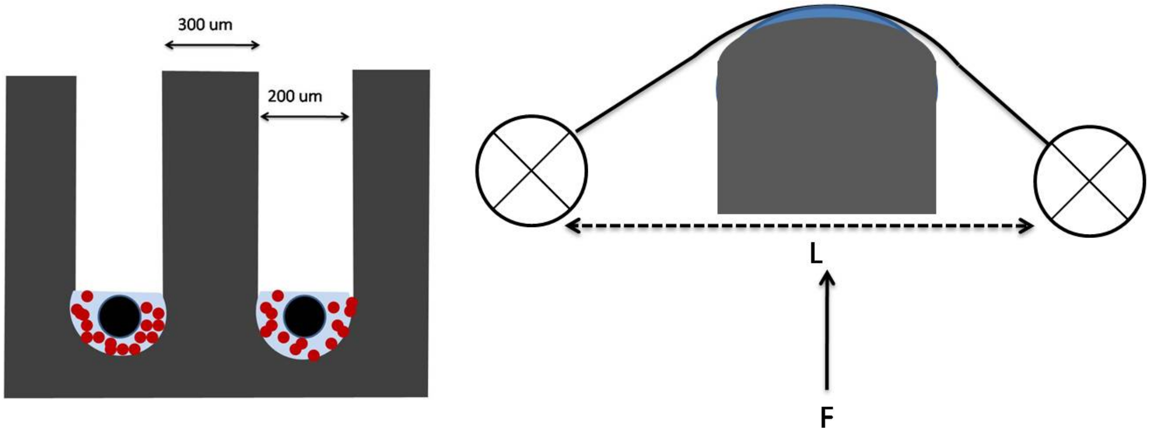

Figure 4: *An illustration of kerf, wafer thickness, and an isolation of a single wire saw system*

Mechanical Planarization (CMP) approach which is often applied in microelectronics polishing. The second time scale is based on the wire dynamics. The wire travels at a speed between 10-15 m/s in a cutting path of 0.1 m and this gives a residence time of about 0.01s. This suggests that the transport and cutting of silicon material is at a time scale 5 orders of magnitude faster than the ingot profile evolution. The wire dynamics, transport and cutting of silicon can be inferred to be at a pseudo-steady state relative to the ingot profile evolution.

The cutting rate is a direct function of distance between the wire and the ingot surface. In this work, the mechanical behavior of the wire is described by a static circular beam. Coupling the cut evolution, wire mechanics, and silicon cutting models will give the dynamic ingot profile, cutting rate, and parameter sensitivity on cutting rate and time required to cut one square ingot.

2.3 Wire Deflection

The wire is modeled as a static circular beam subjected to a force in the axial direction and as well as a distributed load in the transverse direction; a differential element of such a wire is shown in fig. 5. Whenever a distributed transverse force, q, acts upon a body, a shearing force perpendicular to the axis of the body, V, and resisting bending moments, M, in the beam are produced. This creates a deflection that is denoted by y. The axial load or tension, H, causes the body to be in tension.[14] Noting that the stress-strain relationship is linear and the applied stress is below the elastic limit the deflections obey Hooke's law.

From fig. 5, solving for the equilibrium equations for the vertical forces yields:

$$\begin{aligned} \sum F_y = q(x)\Delta x - V + (V + \Delta V) = 0 \\ \frac{\Delta V}{\Delta x} = -q(x). \end{aligned}$$

Taking the limit as Δx approaches zero yields:

$$\frac{dV}{dx} = -q(x). \tag{1}$$

Now taking the sum of the moments around point A yields

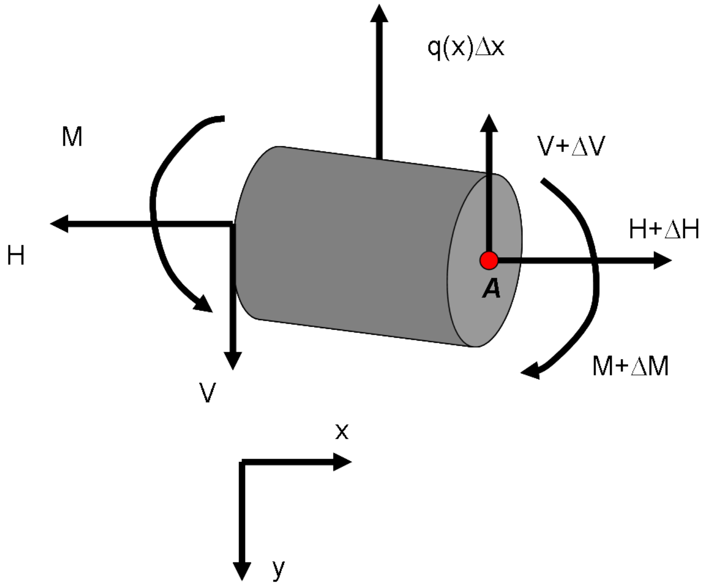

Figure 5: *A differential wire element*

$$\sum M_A = M - (M + \Delta M) + q(x)\Delta x\frac{\Delta x}{2} + V\Delta x + H\frac{\Delta y}{\Delta x}\Delta x = 0$$

Note that the axial tension has been displaced a distance of $(\Delta y/\Delta x)\Delta x$ with respect to the point A and also that on this discrete element the applied load will be taken at the center of the element. The following can be deduced after dividing by Δx

$$-\frac{\Delta M}{\Delta x} + H\frac{\Delta y}{\Delta x} = -q(x)\frac{\Delta x}{2} - V.$$

Taking the limit as Δx approaches zero yields:

$$\frac{-dM}{dx} + H\frac{dy}{dx} = -V. \qquad (2)$$

Differentiating (2) with respect to x with (1) gives

$$-\frac{d^2M}{dx^2} + H\frac{d^2y}{dx^2} = q(x). \qquad (3)$$

From Euler-Bernoulli beam theory, the moment is equal to [14]

$$M = EI\frac{d^2y}{dx^2}. \qquad (4)$$

where E is Young's Modulus and I is the second moment of the area of the cross section. The second moment of the area of circular beams is calculated as

$$I = \pi\frac{R^4}{4}. \qquad (5)$$

Then therefore one can show

$$-EI\frac{d^4y}{dx^4} + H\frac{d^2y}{dx^2} = q(x). \tag{6}$$

This is a fourth order ODE with the following required boundary conditions

$$y(0) = y(L) = \frac{dy}{dx}(0) = \frac{dy}{dx}(L) = 0. \tag{7}$$

At each end of the spool the deflection is zero and the wire fixed and flat. Therefore the slope is equal to zero as well.

2.4 Material Removal

Two modes of contact exist in the channel between the SiC abrasives, wire, and the crystal. The two contact modes are the hydrodynamic contact mode and the solid-solid contact mode. This is depicted in fig. 6. In the hydrodynamic mode, free particles contact the substrate surface randomly and exert a force from the hydrodynamic pressure. This type of material removal is termed three-body abrasion. In solid-solid contact, the abrasive particle is embedded onto the wire and slides along the substrate surface and creates a ploughing effect. With the latter mode being the most substantial mode of material removed.[4] Another mode is the rolling-indenting removal as proposed by Li, et. al where particles rotate and chip away silicon [7].

Mean particle size of the abrasives range from 2-32 μ m [12] and the average film thickness as predicted by Möller is 40 μ m. Because the particle size scales as the film thickness, Möller inferred that the majority of the material removal was in the solid-solid contact. However, Bhagavat et. al. has proposed that the removal is a combination of the three-body removal, rolling-indentation model and solid-solid contact and was calculated using a stochastic simulation. A common characteristic between the models was as the film thickness decreased solid-solid abrasion mode increased and material removed increased. [4-6] The complexity of the various cutting modes gives rise to a more simplified modeling approach.

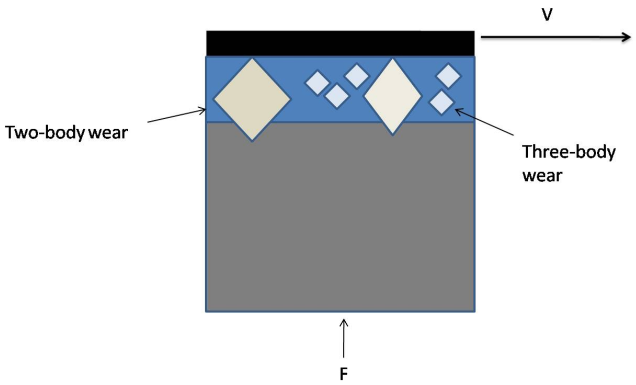

Figure 6: *Illustration of the two major types of wear in the channel*

Our material removal model can be derived from a Chemical Mechanical Planarization (CMP) approach. CMP is a process used in the semiconductor manufacturing industry to polish wafers to create flat mirror finishes for optical materials. The Preston Equation is the most frequently referenced expression for polish rate in CMP. It is based on experimental findings[15-17]. However it was later developed analytically by Brown et. al for purely mechanical wear [17]. The Preston Equation states

$$\frac{\Delta w}{\Delta t} \propto P \frac{\Delta s}{\Delta t} \tag{8}$$

where w is the height of the surface, t is the time, P is the pressure onto the ingot, and $\Delta s/\Delta t$ is the relative velocity between the wire and the ingot. From previous work that has been done in wire saw applications, the material removal rate is a direct function of the film thickness. As the film is decreased the amount of active particles involved in solid-solid abrasion increases. Therefore the distributed load (N/m), F_p, transmitted from the wire to the particles along the length wire is a direct function of the film thickness. If we assume the channel as half a cylinder, the pressure can be formulated as

$$P = \frac{F_p}{1/2 channel circumference} = \frac{2F_p}{\pi D_k}$$

where D_k is the width of the kerf or radius of the channel. The term $\Delta s/\Delta t$ is taken as the mean wire velocity, U. With these definitions, the material removal can be formulated as

$$\frac{\Delta w}{\Delta t} = K_p \frac{2F_p}{\pi D_k} U \tag{9}$$

where K_p is the Preston coefficient which is empirical but for pure solid-solid mechanical abrasion Brown et. al [17] has proven to be analytically equal to

$$K_p = \frac{1}{2E_{substrate}} \tag{10}$$

The term, $E_{substrate}$ is the elastic modulus of the substrate. This expression represents the rate at which the height of the ingot is being removed.

To evaluate the term F_p, the distributed force on top of the SiC abrasives, the spatially changing film thickness and its role in determining the magnitude of the force placed on the SiC particles must be examined. As the slurry film thickness increases the force exerted on particles will decay. The distributed load is also a function of the input load, F, placed on the ingot and therefore F_p can be formulated as

$$F_p = F \frac{e^{-h(x,t)}}{\int_0^{0.3} e^{-h(x,t)} dx} \tag{11}$$

Consider fig. 7, an illustration of the channel, where function y(x,t) is the deflection of the wire and the function w(x,t) is the profile of the ingot. Defining a new function

$$h(x,t) = y(x,t) - w(x,t) \tag{12}$$

This new function *h* will be defined as the film thickness of the channel.

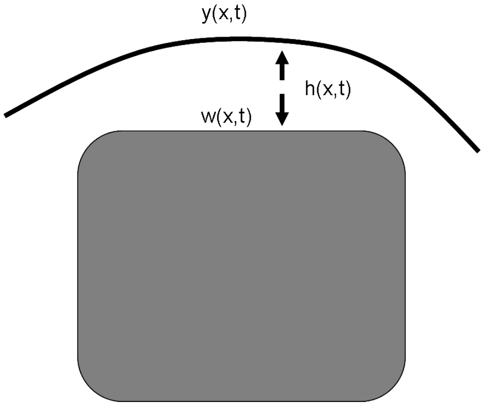

Figure 7: *The film thickness*

2.5 Preston Coefficient

From a detailed scaling analysis of the material removal model, the order of the Preston coefficient can be determined and then compared to the order of the analytically proven coefficient from Brown et. al. First the time required to wafer a 100 x 100 mm^2 block ranges from 4 to 6 hrs [13] and therefore the characteristic time of the process is hours. As stated before the velocity ranges from 10-15 m/s and the order of the velocity is 10. The channel circumference is on order of the kerf which is order of 10^{-4}. The amount, w, cut scales like the total height of the ingot which is on order of 10^{-1}. Lastly, the distributed load scales like a constant distributed uniform load over the cutting length of 0.1 m and this is on order of 10 N/m. From the scaling analysis,

$$\frac{\Delta w}{\Delta t} = K_p \frac{2F_p}{\pi D_k} U$$

$$K_p \approx \frac{\tilde{w} D_k}{\tilde{t} \tilde{U} \tilde{F}_p}$$

where $\tilde{w}$,$\tilde{t}$, $\tilde{U}$, and $\tilde{F_p}$ are all the scaled values. Then the order of the Preston coefficient is

$$K_p \approx \frac{10^{-1}10^{-4}}{360000} \approx 10^{-11}$$

Now the analytic K_p as predicted by Brown et. al with the elastic modulus of 190 GPa[18]. From eq. 10, the predicted Preston Coefficient is $2.63x10^{-12}$. The constant, as predicted by the scaling analysis, is an order faster than the analytic constant.

2.6 Initial Wire Deflection

Initially when the ingot is pushed upon the wire web, much of the distributed load is placed at the ingot edges as the wire is wrapped around the ingot. Figure 8 illustrates the load under these conditions and due to symmetry half of the load is at each edge. An analytical solution is determined first and then compared to the solution determined numerically.

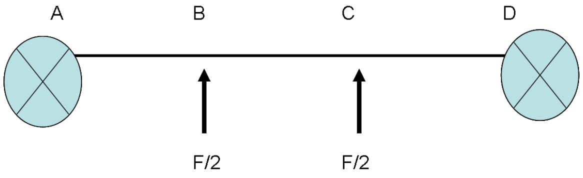

Figure 8: *Inital forces on the wire*

First the necessary force and moment reactions must be determined. Then shear and moment diagrams will be constructed and lastly based on the data gathered, appropriate boundary conditions will be applied to solve the wire BVP. Consider fig. 9 the system has force and moment reactions at the spool ends. Due to symmetry of the point loads at B and C, the force reactions and moment reactions to keep the system static are equivalent in magnitude. The system will be broken into three segments AB, BC, and CD. Force and moment balances will be determined.

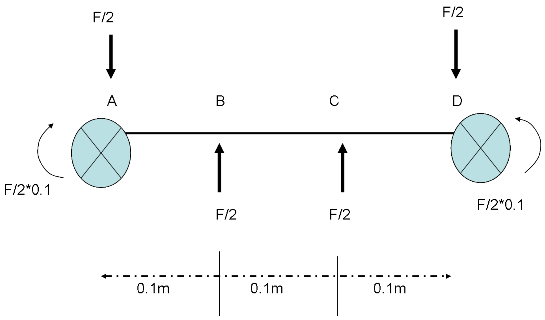

Figure 9: *System after reactions*

2.6.1 Segment AB

In the first segment consider any point in $0 \leq x \leq 0.1$. One must then ask the question: *What are the necessary internal forces to keep the segment of the wire in equilibrium?* Figure 10 shows the segment under question and notice that an upward internal force at A* must exist for the system to be equilibrium. Throughout this segment, the shear force is constant. By convention, an upward internal force, V, acting on a isolated right segment of a beam or a downward force acting on a left segment of a beam corresponds to positive shear. The corresponding shear diagram shows this constant positive shear in

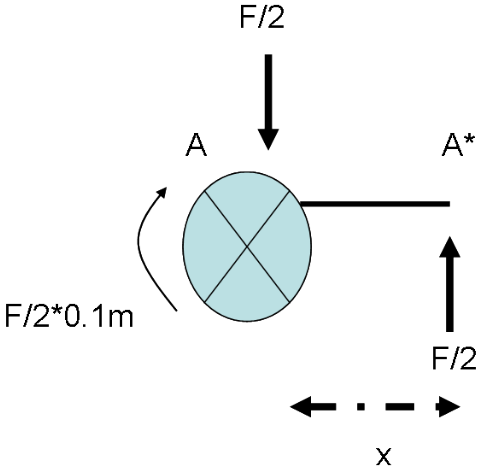

Figure 10: *Segment AB*

fig 11. The sum of the moments around point A* gives:

$$\sum M_{A*} = \frac{F}{2}0.1 - \frac{F}{2}x.$$

Now shear and moment diagrams can be determined. Two conclusions can be made from this analysis. First the moment at 0.1 is equal to zero and the shear force is equal to +F/2. Now consider eq. 6 but the homogeneous version

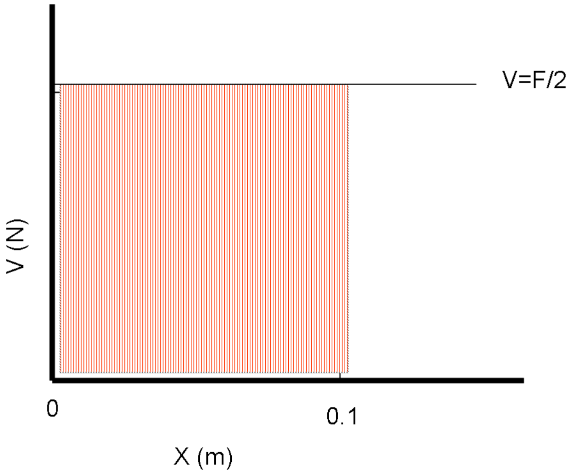

Figure 11: *Shear diagram for segment AB*

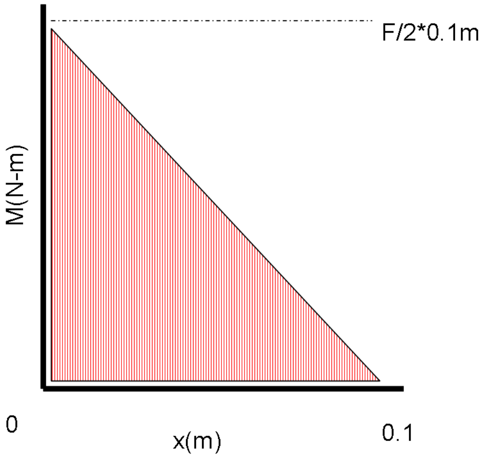

Figure 12: *Moment Diagram for segment AB*

$$-EI\frac{d^4y}{dx^4} + H\frac{d^2y}{dx^2} = 0.$$

This gives the general solution

$$y = A_1 + A_2x + A_3e^{\lambda x} + A_4e^{-\lambda x} \tag{13}$$

where $\lambda = \sqrt{H/EI}$.It is subjected to boundary conditions of the slope equal to zero and the deflection equal to zero at $x = 0$. Now introducing the two pieces of information from the analysis gives rise to two new boundary conditions at $x = 0.1$. First the moment is equal to zero and using eq.4 one can say

$$\frac{d^2y}{dx^2}(0.1) = 0.$$

Lastly, differentiating the homogeneous version of eq. 6 gives a shear force balance throughout the segment. At x=0.1, the shear force is equal to +F/2 and this is the other boundary condition,

$$-EI\frac{d^3y}{dx^3}(0.1) + H\frac{dy}{dx}(0.1) = F/2.$$

2.6.2 Segment CD

A similar analysis can be now be done for the third segment shown in fig 13. Consider any point in $0.2 \leq x \leq 0.3$ and solving for the internal shear force at D* gives F/2. By convention, an downward internal force, V, acting on a isolated right segment of a beam or a upward force acting on a left segment of a beam corresponds to negative shear. Similarly the shear force is constant throughout this segment and it corresponds to -F/2.

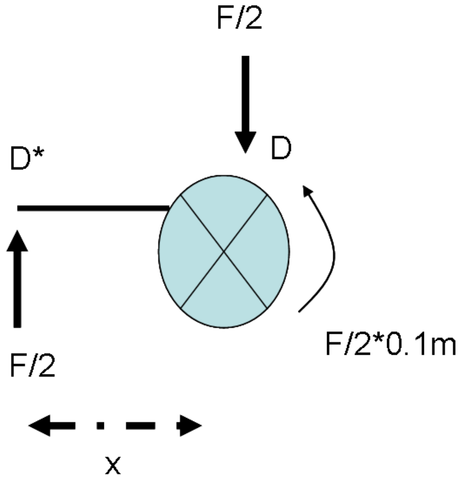

Figure 13: *Segment CD*

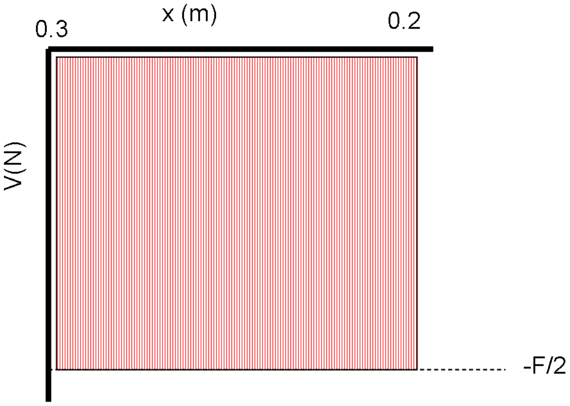

Figure 14: *Shear diagram for segment CD*

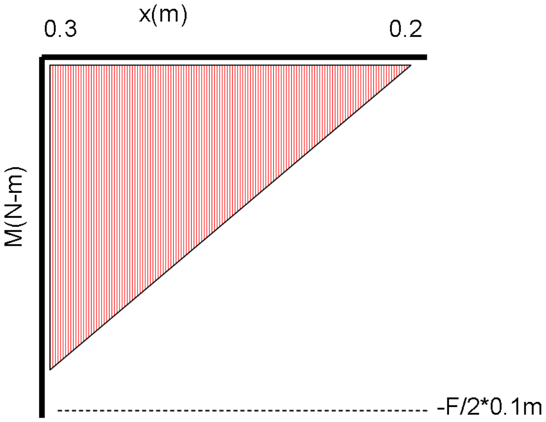

Figure 15: *Moment diagram for segment CD*

Taking the sum of moments around point D* gives

$$\sum M_{D*} = \frac{F}{2}0.1 - \frac{F}{2}(0.3 - x)$$

Shear and moment diagrams diagrams can then be determined. From fig. 14 and 15, the shear force at x=0.2 is equal to -F/2 and the moment is equal to zero at x=0.2. Once again if we solve for the homogeneous BVP throughout this segment another solution is determined with four new unknown constants

$$y = C_1 + C_2 x + C_3 e^{\lambda x} + C_4 e^{-\lambda x}. \tag{14}$$

Using the boundary conditions that the deflection and slope are equivalently equal to zero at x=0.3 we can solve for two constants. Now the last two constants come from the new information from the preceding analysis, the moment is equal to zero at x=0.2 and the shear is equal to -F/2 at x=0.2. Like in the preceding analysis, the second derivative is equal to zero and forming a shear balance gives these two conditions

$$-EI\frac{d^3y}{dx^3}(0.2) + H\frac{dy}{dx}(0.2) = -F/2$$
$$\frac{d^2y}{dx^2}(0.2) = 0.$$

2.6.3 Segment BC

Using the same ODE, a third solution can be defined in $0.2 < x < 0.3$

$$y = B_1 + B_2x + B_3e^{\lambda x} + B_4e^{-\lambda x}.$$

The four boundary conditions to satisfy this problem come from continuity relationships to the outer segment solutions. Therefore the following boundary conditions can be made:

$$y(0.1) = y_{AB}; \frac{dy}{dx}(0.1) = \theta_{AB} \tag{15}$$

$$y(0.2) = y_{CD}; \frac{dy}{dx}(0.2) = \theta_{CD} \tag{16}$$

The first set of boundary conditions simply state that the deflection at x=0.1 is equal to the deflection computed by eq. 13. Similarly the slope at point x=0.1 is equal to the slope computed by eq. 13. An identical treatment is used for the point x=0.2 and eq. 14. Figure 16 shows the composite analytical solution for the initial deflection.

2.7 Numerical Solution

The numerical solution for this fourth order BVP is found by using a collocation spectral method to discretize the differential equation. These collocation points are the zeros of an interpolating polynomial. Figure 17 gives an example of a one-dimensional discretized collocation or quadrature grid. The solution is found by driving the residuals of the BVP at

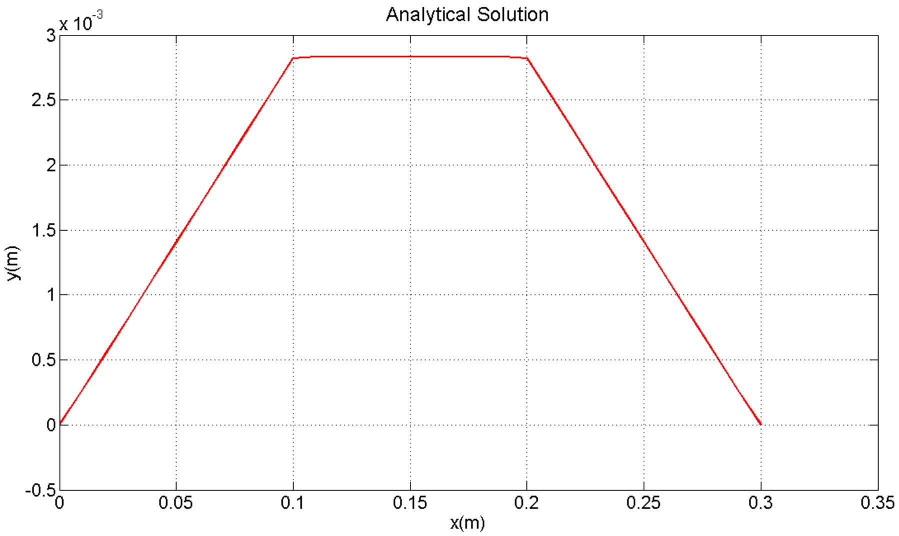

Figure 16: *Analytical Solution for the Initial Deflected Wire*

the collocation points to zero using a Newton-Raphson technique to solve the discretized equations.

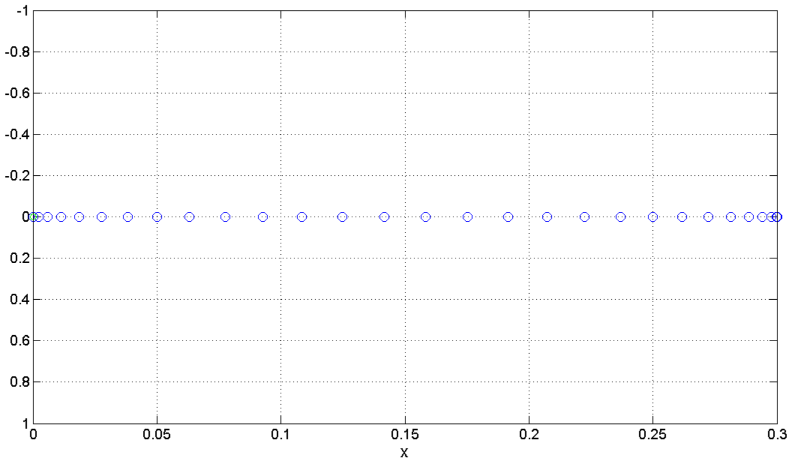

Figure 17: *1-D quadrature grid*

Objected-oriented programming concepts were employed via Matlab to significantly reduce the complexity of these numerical analysis methods.[18]

Now consider again the problem of the initial deflection of the wire. Initially The exerted force is over an infinitesimal amount of area and therefore can be represented by the Dirac delta function. The Dirac delta function is a function often used to model forces applied over a short amount of time or area. An application of this function is the striking of a spring mass system suddenly with a hammer. The properties of this function are:

$$\delta\left(x-a\right)=\begin{cases}\infty, & \text{if } x=a\\ 0, & \text{if } x\neq a\end{cases} \tag{17}$$

$$\int_{-\infty}^{\infty}\delta(x-a)dx=1 \tag{18}$$

Therefore the beam equation can be formulated as:

$$-EI\frac{d^4y}{dx^4}+H\frac{d^2y}{dx^2}=-q(x)=-\frac{F}{2}[\delta(x-0.1)+\delta(x-0.2)] \tag{19}$$

The dirac delta function can be approximated by using the triangle in fig. 18 with an area of F/2. The accuracy of this approximation is increased by making the triangle infinitesimally thin. To employ the problem numerically, two isosceles triangles are produced as in fig. 18 each with an area of F/2.

A numerical solution is calculated with the given expression for the distributed load

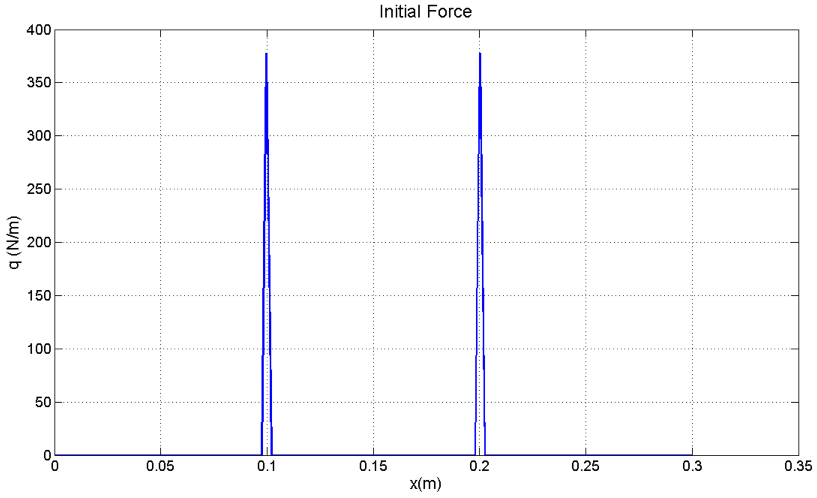

Figure 18: *Initial distributed load*

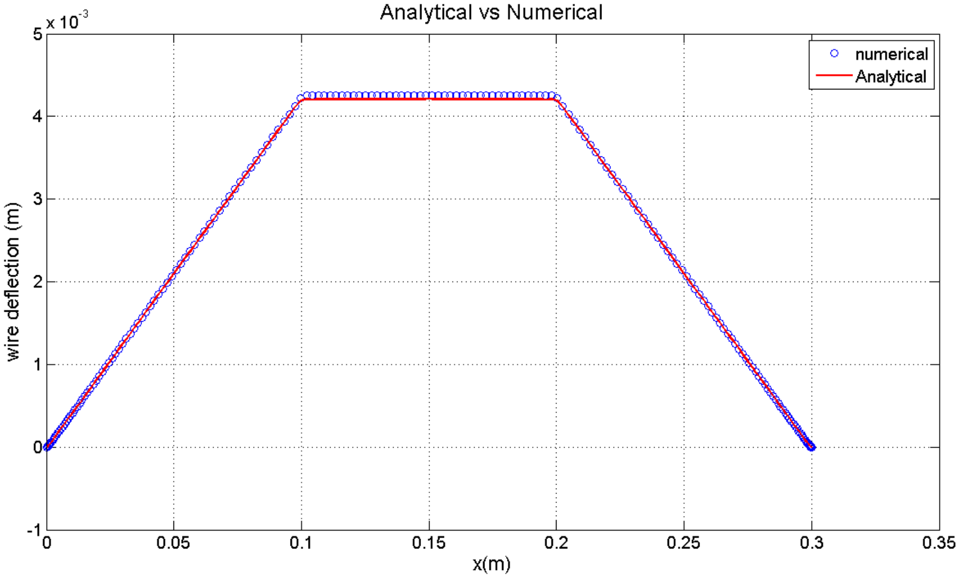

Figure 19: *Numerical and analytical solution for initial deflected wire*

and the four original boundary conditions. Figure 19 shows a comparison of the numerical and analytical solution of the wire deflection. The numerical solution is almost an identical match to the analytical composite solutions because the discrepancy between the numerical and analytical solution is negligible. This validates future dynamic solutions.

The error of the analytical and numerical solution was computed as

$$error = \sqrt{\int_0^{0.3} (Analytical - Numerical)^2 dx} \tag{20}$$

Figure 20 shows the norm of the error versus the number of collocation points is increased. The error analysis shows that the order of the error with even 30 collocation points has an error on the order of 10^{-5}. The optimal amount of collocation steps was found to be 100 points and points above did not show any significant increase in accuracy. The numerical techniques in this analysis validates the full simulation of ingot cutting

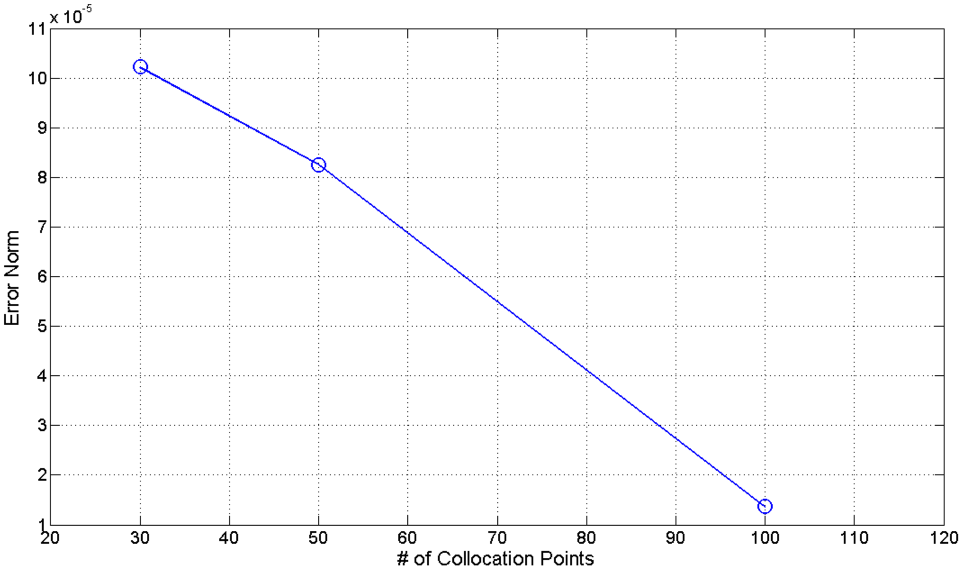

Figure 20: *The norm of the error versus the number of collocation points*

2.8 Numerical Simulation

Initially the flat ingot is pushed against the wire to create the deflection as discussed in the previous section. The edges are removed and this is determined from eq. 9. The ingot is always being pushed against the wire web and therefore the distance between the ingot and wire has to be minimized with the restriction that the film thickness is at least the average size of SiC abrasive. Now since the edges have been removed the distributed load is now dependent on the film thickness and eq. 11 is utilized. A new cutting rate is then determined along with a new deflection of the wire and this algorithm is repeated until the amount removed is 0.1 m.

2.8.1 Ingot Profile Evolution

The slow evolution of the ingot profile, $w(x,t)$, can be determined from a forward Euler finite difference scheme

$$\frac{f(t+\Delta t, x) - f(t, x)}{\Delta t} \approx f'(t, x). \tag{21}$$

Equation 21 can now be rewritten in terms of the ingot profile, w(x,t), and eq. 9 as:

$$w_{n+1}(t,x) = w_n(t,x) + \frac{\Delta w}{\Delta t}\Delta t$$

The time step is 360s.

At each time step a new $h(t,x)$ is calculated and as well as Fp. The dynamics of the wire, ingot surface, film thickness, and force on a particle are recorded for subsequent analysis. Time required to produce a cut as well as a sensitivity analysis can be applied with parameters such as wire tension, normal ingot force and wire velocity.

Chapter 3

3 Results and Discussion

The base case system as described in table 1 will be first be simulated by the given model. The ingot profile evolution will be produced as well as the evolution of the cutting rate. Then a sensitivity analysis with respect to the normal force will be employed to the spatially varying cutting rate. In the next two cases, the wire tension and wire mean velocity will be increased. For each case, the ingot profile, cutting rate, and sensitivity analysis will be simulated at a given time during the cut and compared to the base case. Lastly, the relative cutting times for each case will be produced.

3.1 Base Case

With the values listed in table 1 as the base case situation, numerical results were produced. The ingot profile evolution shows the dynamic nature of the ingot surface. Using a time step of 360s, the time to cut the 100 x 100 mm^2 was approximately 4.3 hrs which is typical for wire saw operations.

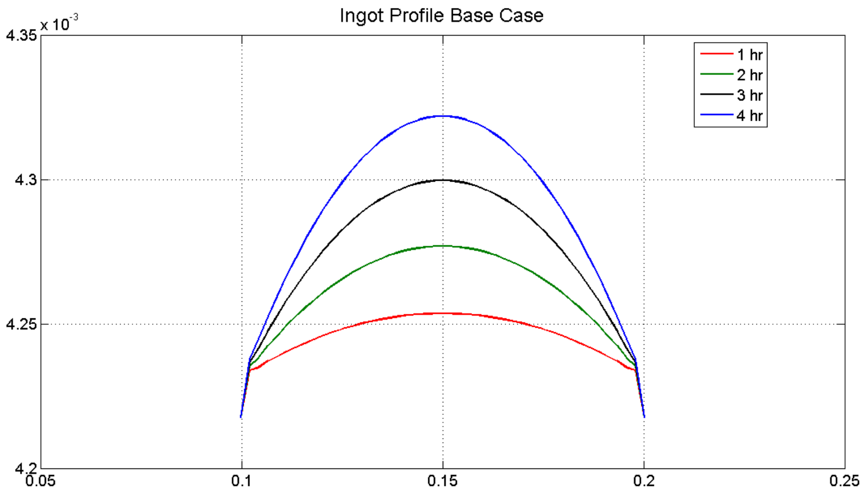

Figure 21: *Dynamic ingot profile*

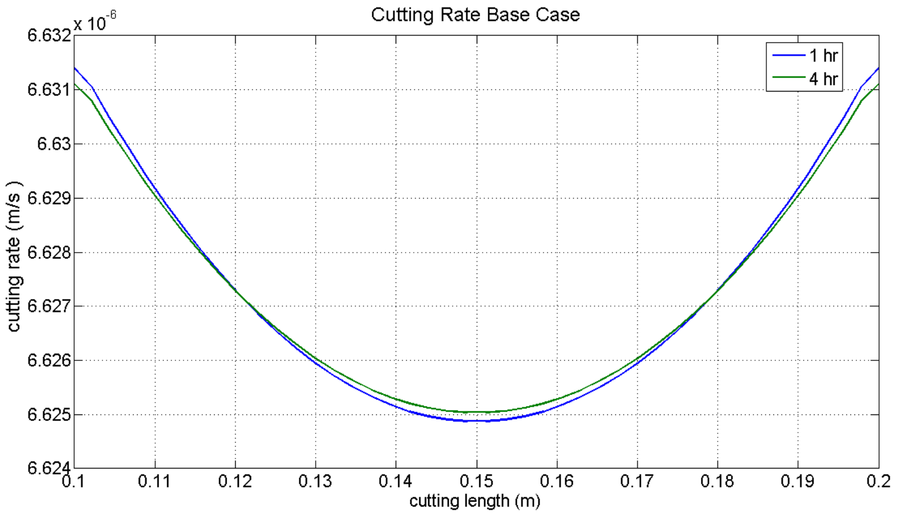

Figure 22: *Cutting rate along the cutting length of the wire for t=1 hr and t=4 hr*

For this particular case, the ingot shape never reaches a steady state and this is due to the slow time scale of the ingot profile evolution. In fig. 21 at each time step the profiles suggest that the ingot surface is approaching the shape of the deflected wire.

Figure 22 considers the cutting rate at t=1hr and t=4hr. At the ends of the ingot the cutting rate is larger and relatively smaller towards the center of the ingot at earlier times. When compared to the cutting rate at t=4hr, the cutting rate towards the end of the ingot are decreased and towards the center the cutting rate has increased. The cutting rate is approaching a constant spatially uniform cutting rate as time passes.

The sensitivity analysis of the cutting rate was based on the upward normal force on the ingot, F. The theory of sensitivity analysis is based on the following [18]. Given a set of linear or nonlinear equations and a single parameter p:

$$\mathbf{r}(z, p) = 0 \ \text{ at } \ \mathbf{z} = \tilde{\mathbf{z}}$$

The set of equations, r, are the residuals that are forced to zero at the collocation points using a Newton-Raphson technique. The solution $\tilde{\mathbf{z}}(\tilde{p})$ for $p = \tilde{p}$. The sensitivity is defined as:

$$\mathbf{S}(\tilde{p}) = \frac{d\tilde{\mathbf{z}}}{dp}|_{\tilde{p}}$$

This is the rate of change of the state variable with respect to the parameter p. In fig. 23 the small perturbations of the normal force applied affects the cutting rate greatest at the ends at t=1 hrs and decreases towards the center of the ingot profile. As time passes the sensitivity of the cutting rate becomes uniform.

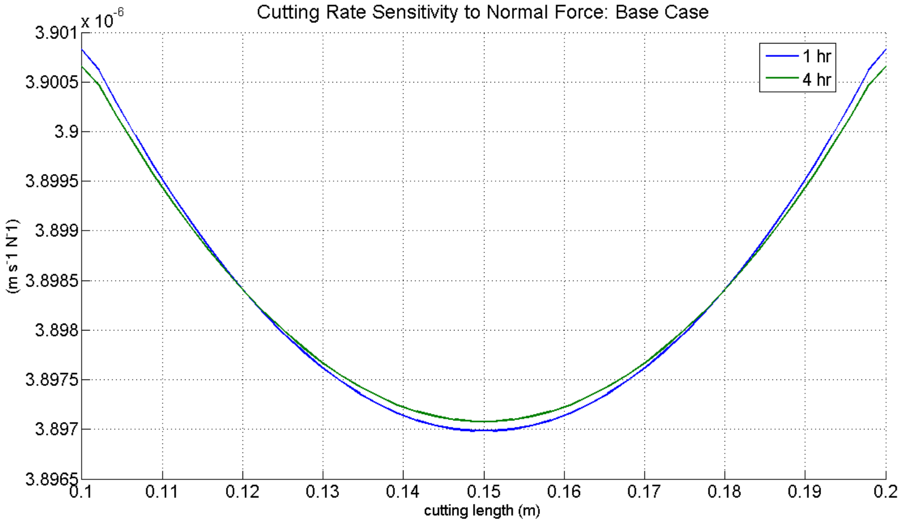

Figure 23: *Sensitivity of cutting rate with respect to the normal force along the cutting length of the wire for t=1 hr and t=4 hr*

3.2 Increased Tension

One real-time parameter that is controlled and can be adjusted is the internal tension of the wire. In this system the tension of the wire was adjusted to 28 N which is a 40 percent increase. Figure 24 depicts the final deflection of the wire for the base case and the increased tension case. With this increased tension a flatter wire deflection is produced. The ingot profile midway through the base case cut is given in fig. 25.

With the given profile, instantaneous cutting rate values were produced and compared to the base case values at the identical time of 2hrs. From the predicted model, the increased tension suggests a more uniform cutting rate spatially. At the ends of the ingot, the increased tension system has a lower cutting rate relative to the base case. Also towards the center of the ingot, the increased tensioned system has an increased cutting rate relative to the base case. However, the increase does not affect the time required to cut through the square ingot. Like in the base case the time required to cut was 4.3 hrs.

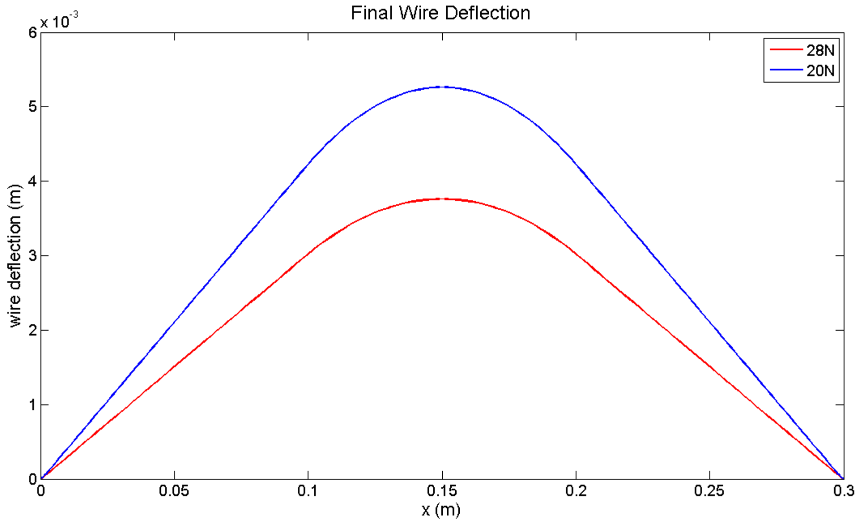

Figure 24: *Deflection of wire for H=28N and H=20N*

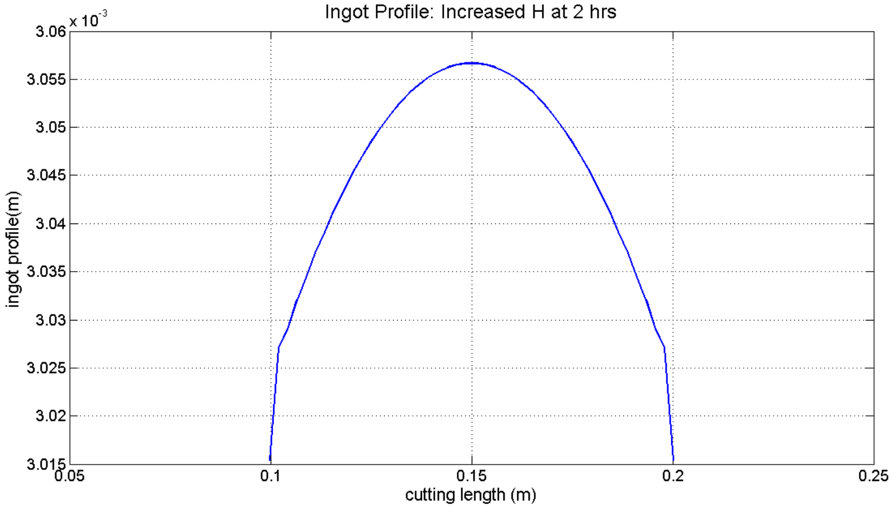

Figure 25: *Ingot Profile for Increased Tension Case for t=2hr*

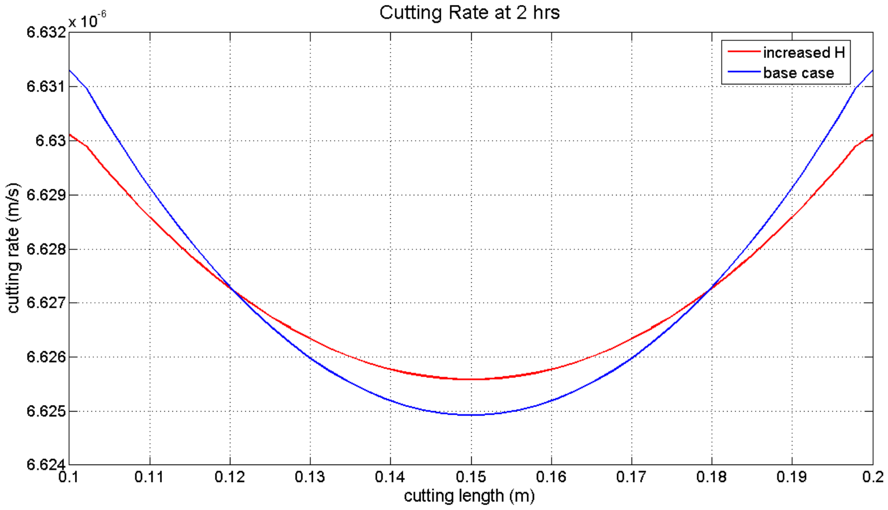

Figure 26: *Cutting rate comparison for Increased Tension and Base Case for t=2hr*

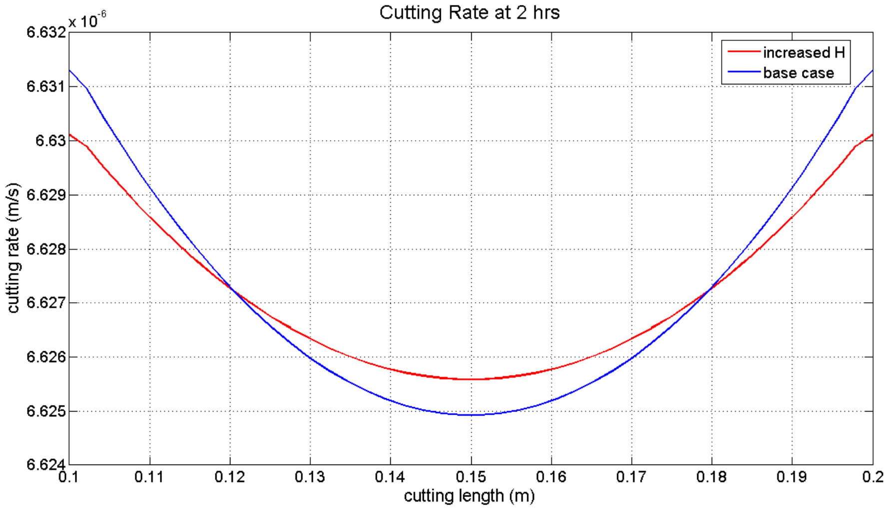

Figure 27: *Sensitvity Analysis Comparison for Increased Tension and Base Case for t=2hr*

A normal force sensitivity analysis was also determined for the increased tensioned case and compared with the base case. This is depicted in fig. 27. Small perturbations of the normal force remove more material at localized points at the ends of the ingot and remove less material at points towards the center of the ingot. This suggests having a higher tensioned system can provide a more uniform cut and an even distribution of the force applied. This prevents the possibility of wire breakage at local high pressured points.

3.3 Increased Velocity

Wire velocity is typically maintained between 10-15 m/s. With an increase in velocity of 20 percent, the time required to cut through the block was 3.6 hrs. Figure 28 illustrates the profile of the ingot at 2 hrs for the base case and the increased velocity case. The increased velocity case depicts an accelerated profile because the time scale of the ingot profile evolution has been lowered with this increase of velocity. In addition fig. 29 shows the increased cutting rate at t=2hr. When compared to the base case cutting rate, the increased velocity causes an average increase of 20 percent in the cutting rate.

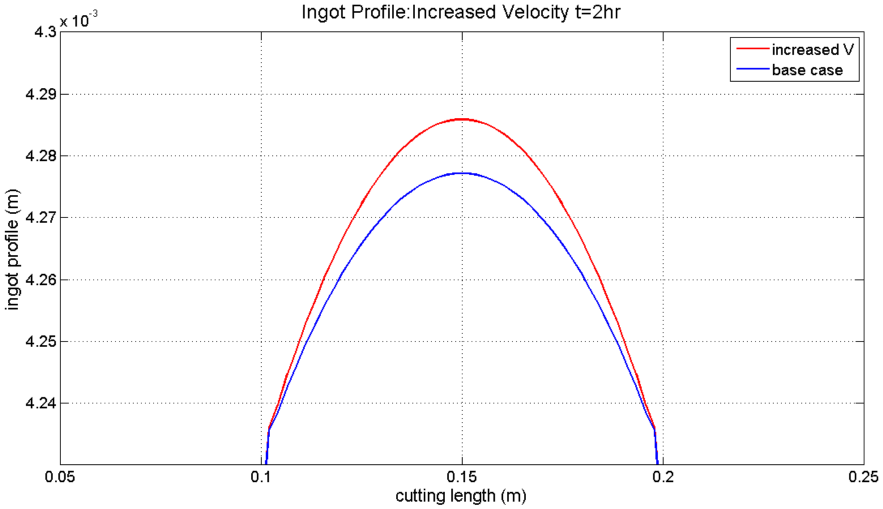

Figure 28: *Comparison of Ingot Profile for Increased Velocity and Base Case for t=2hr*

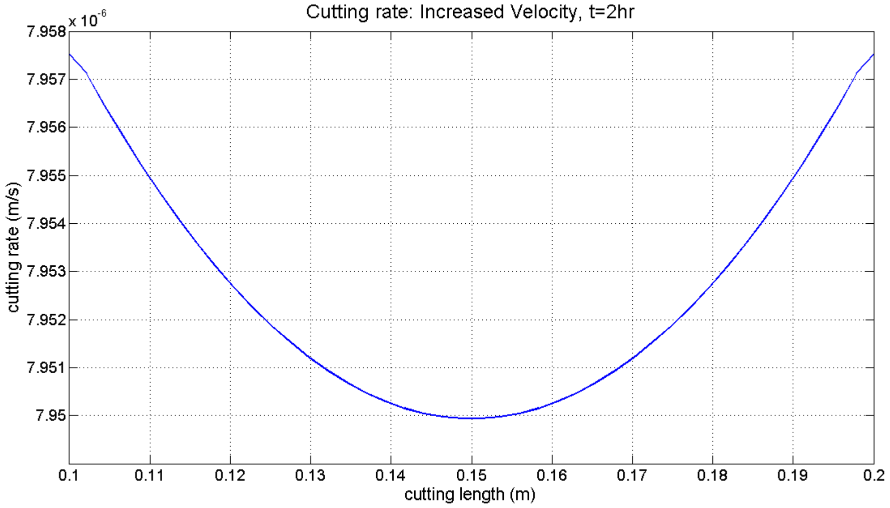

Figure 29: *Cutting Rate for Increased Velocity Case*

Table 2: Cutting Times

Case	Time Required
Base Case	4.3 hr
Increased H	4.3 hr
Increased U	3.6 hr

From these three cases, the cutting rates along the wire were determined and as well as the sensitivity to the normal force. During the wire saw process careful control of the cutting rate along the wire length is one of the factors that determine the quality of the wafer surface. In cases where film thickness is of the same order as the abrasive size, ploughing of the material by the trapped abrasive dominates. In this mode of removal, silicon is being chipped away and is susceptible to cracks. Uniformity of the cutting rate along the wire is ideal to avoid localized regions of relative high removal rate which can lower the surface quality of the final wafer. Surface quality refers to non-uniform surface height and formation of saw ridges. With our analysis, a higher tension system is ideal since an increase in the wire tension promotes uniform cutting rates along the cutting length. Also lower operating times are desired to increase throughput, lower the consumption of SiC slurry, and decrease electrical usage. A summary of cutting times is listed in table 2.

Increasing the velocity from 10 m/s to 12 m/s has lowered the time to slice one ingot by 20 percent.

Chapter 4

4 Conclusions and Future Work

In this project, the wire saw system was developed integrating the basic physics of the wire through the fourth order static beam equation and a CMP model for material removal. A base case system was established typical of industry applications. In this starting analysis of the silicon slicing operation, a model was established describing the removal rates as a function of time and the cutting length. Using a simplified approach to describe the relationship between film thickness and the distributed load on the abrasive particles, realistic results were achieved in the simulation. From this model, the ingot profile evolution was characterized by a slow time scale on the order of hours. The main finding in this study was that relevant parameters in the system like wire tension and wire velocity can be manipulated to achieve uniform cutting rates as well as a decreased cut time. Controlling the cut rates in the wire system is paramount in the wire saw application for obtaining good wafer quality and short cut times.

Extensive work in this area is required. The analysis in this project is preliminary and numerous issues need to be answered still. The following issues need to be addressed

- Experimental studies need to be addressed to verify the limits of parameters like wire tension and velocity and as well as to verify the findings found in this project.
- A vibrational analysis of the wire must be determined and its effect on the surface quality on the finished wafer.
- A three-dimensional model of the cutting channel needs to be implemented to study the drag and normal force at the side edges. Then investigate the possibility of an asymmetric hydrodynamic pressure distribution along the cutting length.

- Following in line with the last statement, a model describing the stochastic two-body abrasion for particles that are free floating. These free floating particles remove material by the hydrodynamic pressure applied to it.
- Lastly model regions of the ingot where ingot defects exist. This introduces the possibility of wire breakage and regions of lowered material removal.

References

[1] N. G. Dhere, Toward GW/year of CIGS production within the next decade, *Solar Energy Materials and Solar Cells* **91** 1376-1382 (2007).

[2] A Goetzberger,C. Hebling, Photovoltaic materials, past, present, future, *Solar Energy Materials and Solar Cells* **62** 1-19 (2000).

[3] A. Mueller, N. Cherradi, P. M. Nasch, The Challenge To Implement Thin Wafer Potenital With Wire Saw Cutting Technology, *3rd World Conference on Photovoltaic Energy Conversion May 11-18, 2003 Osaka. Japan* 1477-1478.

[4] J. Wohlgemuth,M. Narayanan, Large-Scale PV Module Manufacturing Using Ultra-Thin Polycrystalline Silicon Solar Cells Annual Subcontract Report 1 October 2003 September 2004,National Renewable Energy Laboratory

[5] H. J. Möller, Wafering of silicon crystals, *phys. stat. sol. (a)* **4** 659 (2006).

[6] M. Bhagavat,V. Prasad, I. Kao, Elasto-Hydrodynamic Interaction in the Free Abrasive Wafer Slicing Using a Wiresaw: Modeling and Finite Element Analysis, *Transactions of the ASME* **122** 394 (2000).

[7] H. J. Möller,C. Funke, M. Rinio, S. Scholz, Multicrystalline silicon for solar cells, *Thin Solid Films* **487** 179 (2005).

[8] J. Li,, I. Kao,V. Prasad, , Modeling Stresses of Contacts in Wire Saw Slicing of Polycrystalline and Crystalline Ingots: Application to Silicon Wafer Production, *Transactions of the ASME* **122** 394 (2000).

[9] M. Bhagavat,I. Kao, A finite element analysis of temperature variation in silicon wafers during wiresaw slicing,*International Journal of Machine Tools and Manufacture* **48** 95-106 (2008).

[10] J. Yamada,, F. Kinai,T. Ichikawa,A. Yokoyama, M. Fukunaga, T. Ohshita , Warpage analysis of Silicon Wafer in Ingot Slicing by Wire-Saw Machine, *MATERIALS PROCESSING AND DESIGN: Modeling, Simulation and Applications - NUMIFORM 2004 - Proceedings of the 8th International Conference on Numerical Methods in Industrial Forming Processes* **712** 1459-1463 (2004).

[11] G. Du, L. Zhou, P. Rossetto,Y. Wan, Hard inclusions and their detrimental effects on the wire sawing process of multicrystalline silicon, *Solar Energy Materials and Solar Cells* **91** 1743 (2007).

[12] X. Sun, Z.J. Pei, X.J. Xin, M. Fouts, Waviness removal in grinding of wire-sawn silicon wafers: 3D finite element analysis with designed experiments, *International Journal of Machine Tools and Manufacture* **91** 1119 (2004).

[13] L. Zhu, I. Kao, Galerkin-based modal analysis on the vibration of wireslurry system in wafer slicing using a wiresaw, *Journal of Sound and Vibration* **283** 589 (2005).

[14] Popov, E.P. (1990). *Engineering Mechanics of Solids*. New Jersey: Prentice Hall.

[15] Steigerwald, J.M., Murarka, S.P., Gutman, R.J. (1997). *Chemical Mechanical Planarization of Microelectronic Materials*. New York: Wiley.

[16] Luo, J., Dornfeld, D.A. (2004). *Integrated Modeling of Chemical Mechanical Planarization for Sub-Micron IC Fabrication*. New York: Springer.

[17] N.J. Brown, P.C. Baker, R.T. Maney, M. Fouts, Optical polishing of metals, *SPIE* **306** 16 (1981).

[18] Franssila, S. (2004). *Introduction to Micro Fabrication.* London: Wiley.

[19] Adomaitis, R.A. (2007). *Numerical Methods for Chemical Engineers: An object-oriented, MATLAB based approach.* College Park: University of Maryland.